Brownian dynamics simulations for the narrow escape problem in the unit sphere

Vaibhava Srivastava[1,*] and Alexei Cheviakov[2,†]

[1]*Department of Mathematics, Iowa State University, Ames, Iowa 50011, USA*
[2]*Department of Mathematics and Statistics, University of Saskatchewan, Saskatoon, Saskatchewan S7N 5E6, Canada*

The narrow escape problem is a first-passage problem that concerns the calculation of the time needed for a Brownian particle to leave a domain with localized absorbing boundary traps, such that the measure of these traps is asymptotically small compared to the domain size. A common model for the mean first-passage time (MFPT) as a function of particle's starting location in a given domain with constant diffusivity is given by a Poisson partial differential equation subject to mixed Dirichlet-Neumann boundary conditions. The primary objective of this work is to perform direct numerical simulations of multiple particles undergoing Brownian motion in a three-dimensional spherical domain with boundary traps, compute MFPT values by averaging Brownian escape times, and compare these with explicit asymptotic results obtained previously by approximate solution of the Poisson problem. A close agreement of MFPT values is observed already at 10^4 particle runs from a single starting point, providing a computational validation of the Poisson equation-based continuum model. Direct Brownian dynamics simulations are also used to study additional features of particle dynamics in narrow escape problems that cannot be captured in a continuum approach, such as average times spent by particles in a thin layer near the domain boundary, and effects of isotropic vs anisotropic near-boundary diffusion.

I. INTRODUCTION

Since 1827 when Robert Brown first observed random motion of pollen grains in fluid, the concept of Brownian motion and its statistical models has found applications in multiple areas of sciences, from statistical physics to chemistry, molecular biology, neuroscience, and engineering. An important class of problems related to the statistics of randomly moving particles is the first-passage problems where one needs to calculate the average time required by a particle to escape or enter a given domain. The narrow escape problem is a first-passage problem for a domain containing volume or boundary traps, and otherwise impermeable boundary, such that the measure of these traps is small compared to, respectively, the domain volume or boundary measure (see Fig. 1). Narrow escape problems have significant applicability in chemical and biological models, including the diffusion of ions in biological microdomains [1], receptor trafficking in a synaptic membrane [2], of narrow escape kinetics in chemical processes [3], nanoparticle diffusion within inverse opals and related artificial materials with cavities [4], RNA transport in cells and cell nuclei [5], and dynamics of predator-prey interaction in ecosystems [6].

Let $\{W(t)\}_{t\geqslant 0}$ denote a Brownian particle trajectory restricted within a two- or three-dimensional bounded domain Ω. Assume the boundary of the Ω, $\partial\Omega = \partial\Omega_a \cup \partial\Omega_r$ is nearly everywhere reflecting (denoted by $\partial\Omega_r$), except for finitely

many small absorbing windows or regions, each centered at $x_j \in \partial\Omega$, for $j = \{1, 2, \ldots, N\}$, collectively denoted $\partial\Omega_a$, through which particles can leave Ω. A schematic of such problem is shown in Fig. 1.

The mean first-passage time (MFPT) $v(x)$ is defined as the expected value of time required for particles with Brownian trajectories $\{W(t)\}_{t\geqslant 0}$ to escape through one of the boundary traps when launched from $x = W(0)$. In $d = 2$ or 3 dimensions, for asymptotically small absorbing windows $|\partial\Omega_a| = O(\epsilon^{d-1})$, where $0 < \epsilon \ll 1$ denotes the dimensionless radius of the absorbing window, the problem of the calculation of the MFPT $v(x)$ becomes a narrow escape problem. Since as $\epsilon \to 0$, $v(x) \to \infty$ for all starting points $x \in \Omega$, this is a singular perturbation problem.

In the case of constant diffusivity, a continuum model describing the MFPT $v(x)$ in a given domain with boundary traps is given by a Poisson partial differential equation (PDE) with zero Dirichlet (absorbing) boundary conditions $v = 0$ on $\partial\Omega_a$, and Neumann (reflective) boundary conditions $\partial_n v = 0$ on $\partial\Omega_r$ [2,7,8]:

$$\Delta v = -\frac{1}{D}, \quad x \in \Omega,$$
$$v = 0, \quad x \in \partial\Omega_a = \bigcup_{i=1}^{N} \partial\Omega_{\epsilon_i}, \qquad (1.1)$$
$$\partial_n v = 0, \quad x \in \partial\Omega_r,$$

where Δ is the Laplacian operator, and D is the constant diffusivity. The MFPT averaged across all starting positions $x \in \Omega$ are

$$\bar{v} = \frac{1}{|\Omega|} \int_\Omega v(x)\, dx, \qquad (1.2)$$

---

*Corresponding author: vaibhava@iastate.edu
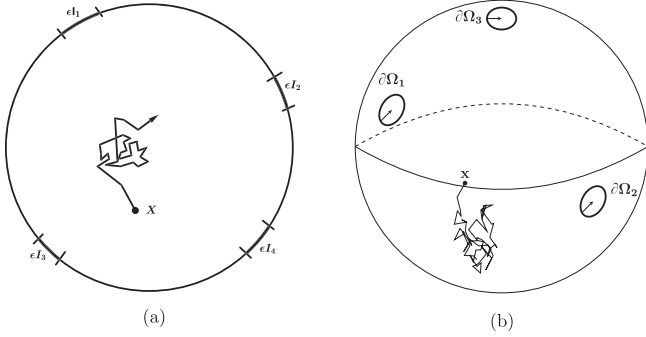†Alternative English spelling: Alexey Shevyakov; shevyakov@math.usask.ca

FIG. 1. (a) Schematics of the narrow escape problem in a two-dimensional spaces having surface traps of length $\{\epsilon I_j\}_{j=1}^4$. (b) Illustration of the three-dimensional narrow escape problem in the unit sphere having circular absorbing windows $\{\partial\Omega_j\}_{j=1}^3$.

where a uniform distribution of initial points x is assumed, provides an integral characteristic of escape dynamics from a given domain with a prescribed trap arrangement.

While the PDE in (1.1) is linear, the complexity of heterogeneous boundary conditions does not allow for common linear PDE techniques to be used to solve the problem exactly, except for single-trap problems in simplest geometries. Approximate asymptotic solutions in the case of small traps of size $\epsilon \ll 1$ have been developed for generic two- and three-dimensional domains with a single trap, as well as for circular, near-circular, and elliptic domains in two dimensions, and a spherical domain in three dimensions [2,9–13]. The leading terms of $v(x)$ and $\bar{v}$ as functions of ϵ are singular as $\epsilon \to 0$. Matched asymptotic expansions were used to compute higher-order terms that depend on trap arrangements through pairwise energy-like terms [11–13], allowing for global optimization of trap locations (see, e.g., Refs. [13–15]). The quality of approximation provided by such asymptotic solutions was studied through comparisons with numerical solutions [16]. Asymptotic solutions of (1.1) for some three-dimensional nonspherical domains have been studied in Ref. [17]. Matched asymptotic expansions were used in Ref. [18] to approximately solve the narrow escape problem in domains with a long neck. First-passage times in moving traps were considered in Refs. [19,20]. Reference [21] used a combination of asymptotic and numerical methods to study affects of curvature and trap clustering in problems involving surfaces with absorbing pores. Brownian statistics in randomly moving receptors on cell surface and the resulting increased association rates were studied in Ref. [22]. Effects of fluctuating diffusivity and gating were considered in Ref. [23]. Reference [24] formulates a framework to quantify the role of surface receptor organization, in particular, clustered receptor configurations, in the ability of a cell to infer the location of an external stimulus.

The benefit of the continuum formulation (1.1) of the narrow escape problem is the applicability of standard PDE methods of analysis and solution, including numerical methods and approximate techniques. However, the solution $v(x)$ does not contain information about particular particle trajectories. Moreover, very few exact or approximate analytical solutions of (1.1) and similar continuum-type models are

known for nontrivial domain geometries, cases of variable and/or anisotropic diffusivity D, etc. It is also well known that the diffusion dynamics changes near a reflective domain boundary, resulting in different normal and tangential diffusion coefficients in the close vicinity of the wall [25]. In Refs. [25,26], models for anisotropic variable diffusion coefficients (in tangential and normal directions relative to the domain surface) for spherical particles were presented in terms of expansions in a/z, where a is the particle radius, and z is the distance to the boundary. In the limit $a/z \to 0$, both diffusion coefficients tend to the same isotropic diffusion value; direct microscopy-based measurements show good agreement with theoretically predicted diffusion coefficients. A different continuum model involving isotropic but variable (piecewise-constant) diffusivity in the radial direction in a disk, inspired by the spatial organization of the cytoskeleton in cells, was studied in Ref. [27], where modified formulas for the MFPT in narrow escape and thin outer shell limits were derived, and effects of various diffusivity ratios were investigated.

A important related topic is surface-mediated diffusion which, in combination with bulk diffusion, leads to two-state (surface vs bulk) paths of Brownian particles, with diffusivity properties that can significantly differ. The corresponding modified first-passage problems properties have been studied in various settings and theoretical assumptions, including surface or bulk diffusion controlled by an internal clock (see, e.g., Ref. [28] and references therein). Other modifications of the escape problem include taking into account force fields that can model forced diffusion due to interactions of macromolecules or cellular organelles with internal structures of the cell [29], surface or bulk diffusion with imperfect adsorption steps where the traveling particle can bounce several times before being adsorbed into the boundary surface, and other generalizations, leading to continuum escape problem formulations different from the simple model (1.1). Such models allow to analyze, for example, particle desorption (transfer) probabilities from the boundary surface to the domain bulk, and relative benefits of surface vs bulk excursions for Brownian particles to optimize escape rates (see, e.g., Refs. [30,31] and references therein).

The objectives of this work is to perform a direct numerical study of multiple particles undergoing simulated Brownian motion inside a three-dimensional spherical domain with boundary traps. First, MFPT values are computed by averaging of Brownian escape times, and are compared to the results predicted by asymptotic solutions of (1.1) (Sec. II). This comparison, which overall shows a good agreement, in some sense validates the PDE formulation (1.1) of the narrow escape problem as an approximation of the averaging of the multiple physical Brownian motion runs. Brownian motion parameters, as well as the number of single-particle launches from a given domain point required to match the predicted asymptotic averaged MFPT values, are estimated. Second, having multiple simulated Brownian trajectories at our disposal, we study the relative times spent by Brownian particles in bulk compared to time spent in a narrow δ-region near the domain boundary (Sec. III). It is shown that particles spend more in the boundary layer than predicted by the boundary layer relative volume, with the effect being more pronounced in a narrow layer near the spherical wall. Finally, the sim-

ulation is modified to take into account anisotropic variable diffusion [25,26] that is a better physical approximation in close proximity to the domain wall. Effects of this diffusion variability and anisotropy on the escape times (MFPT) and time spent near the boundary are studied. It is found that accounting for the modified near-wall diffusion leads to smaller escape times than predicted by the PDE model (1.1), and a larger time spent by particles near the boundary (Sec. IV). We note that the current study considers only the motion within the bulk of the spherical domain, and does not model two-state Brownian trajectories that include purely surface-bound diffusion. The paper is concluded with a summary of the work and some open problems (Sec. V).

All numerical computations have been performed with a `MATLAB`-based code [32] developed in the current work.

II. COMPARISON OF ASYMPTOTIC AND BROWNIAN SIMULATION RESULT FOR THE THREE-DIMENSIONAL UNIT SPHERE

A. Asymptotic formulas and results for the mean first-passage times

An approximate asymptotic solution of the problem (1.1) in the case of an arbitrary number N of small well-separated boundary traps of generally nonequal radii ϵa_j, $\epsilon \ll 1$, was derived in Ref. [12] using the method of matched asymptotic expansions. The solution $v(x)$ was represented by a series $v(x) = v_0 + v_1 + v_2 + \cdots$ in the bulk of the domain away from each trap center x_j, and by a different expansion $v(x) = u(y) = u_0 + u_1 + u_2 + \cdots$ in terms of local stretched variable $y = \epsilon^{-1}(x - x_j)$ when $|x - x_j| \sim O(\epsilon)$. The local and global perturbation series were matched in the overlap region $y \gg 1$, $x \to x_j$, yielding the leading order and subsequent terms

$u_0 = O(\epsilon^{-1})$, $u_1 = O(\log \epsilon)$, $u_2 = O(1)$, calculated using the Neumann-Green function $G(x; \xi)$ satisfying

$$\Delta G = \frac{1}{|\Omega|}, \quad x \in \Omega;$$

$$\partial_n G = 0, \quad x \in \partial\Omega \setminus \{\xi\}; \quad \int_\Omega G \, dx = 0. \quad (2.1)$$

The above PDE admits a unique solution for the domain $\Omega \subset \mathbb{R}^3$ with a smooth boundary; this solution has a known singularity behavior as $x \to \xi$ (cf. Ref. [33]):

$$G(x; \xi) = \frac{1}{2\pi |x - \xi|} - \frac{H_m}{4\pi} \log |x - \xi| + R(\xi; \xi), \quad (2.2)$$

where H_m is the mean curvature of the boundary at $\xi \in \partial\Omega$, and $R(\xi; \xi)$ represents the regular part of $G(x; \xi)$. For the unit sphere domain, one has

$$G_s(x; \xi) = \frac{1}{2\pi |x - \xi|} + \frac{1}{8\pi}(|x|^2 + 1)$$
$$+ \frac{1}{4\pi} \log\left(\frac{2}{1 - |x|\cos\gamma + |x - \xi|}\right) - \frac{7}{10\pi}, \quad (2.3)$$

where γ is the angle between the vector $x \in \Omega$ and $\xi \in \partial\Omega$, $|\xi| = 1$, and

$$R(\xi; \xi) = -\frac{9}{20\pi}. \quad (2.4)$$

For $\epsilon \to 0$, in the outer region $|x - x_j| \gg \epsilon$, the leading-order behavior of the MFPT $v(x)$ solving (1.1) is given by

$$v(x) = \bar{v} + \sum_{i=1}^{N} \kappa_j G(x; x_j) + O(\epsilon), \quad (2.5)$$

where the average MFPT $\bar{v}$ equals

$$\bar{v} = \frac{|\Omega|}{2\pi \epsilon D N \bar{c}} \left[1 + \epsilon \log\left(\frac{2}{\epsilon}\right) \frac{\sum_{j=1}^{N} c_j^2}{2N\bar{c}} + \frac{2\pi\epsilon}{N\bar{c}} p_c(x_1, \ldots, x_N) - \frac{\epsilon}{N\bar{c}} \sum_{j=1}^{N} c_j \kappa_j + O(\epsilon^2) \right] \quad (2.6)$$

in (2.5) and (2.6), $\kappa_j = (c_j/2)(2\log 2 - 3/2 + \log a_j) = \text{const}$, c_j is the trap capacitance (related to the same notion in electrostatics; in particular, $c_j = 2a_j/\pi$ for a circular trap), and $\bar{c} = (c_1 + \cdots + c_n)/N$ is the average trap capacitance. A rigorous proof of (2.5) and (2.6) [34] has provided a sharper estimate $O(\epsilon)$ of the higher-order expansion terms.

In the leading order, the average MFPT (2.6) is inversely proportional to ϵ. The sub-leading term contains the pairwise energy-like trap interaction contribution

$$p_c(x_1, \ldots, x_N) = \mathcal{C}^T \mathcal{G}_s \mathcal{C},$$

defined in terms of the capacitance vector $\mathcal{C} = (c_1, \ldots, c_N)^T$ and the constant $N \times N$ Green's matrix

$$\mathcal{G}_s \equiv \begin{pmatrix} R & G_{s12} & \ldots & G_{s1N} \\ G_{s21} & R & \ldots & G_{s2N} \\ \vdots & \vdots & \ddots & \vdots \\ G_{sN1} & \ldots & G_{sN,N-1} & R \end{pmatrix}, \quad R \equiv R(x_j; x_j) = -\frac{9}{20\pi} \quad (2.7)$$

depending on trap sizes and positions. For N equal traps, the asymptotic average MFPT (2.6) simplifies to

$$\bar{v} = \frac{|\Omega|}{4\epsilon D N} \left[1 + \frac{\epsilon}{\pi} \log\left(\frac{2}{\epsilon}\right) + \frac{\epsilon}{\pi}\left(-\frac{9N}{5} + 2(N-2)\log 2 + \frac{3}{2} + \frac{4}{N}\mathcal{H}(x_1, \ldots, x_N) \right) + O(\epsilon^2) \right], \quad (2.8)$$
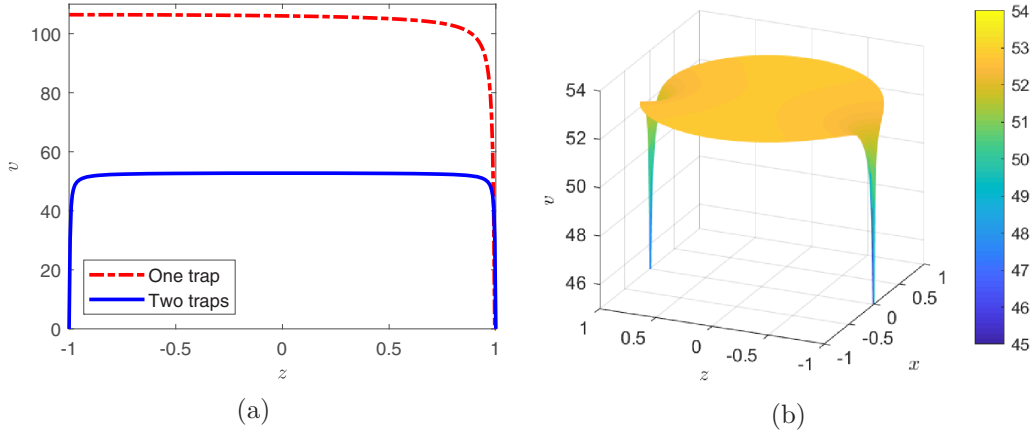
FIG. 2. (a) The asymptotic MFPT (2.5) (2.8) for the unit sphere, along the z-axis, in the case of one and two surface traps of radius $\epsilon = 0.01$, located at $(0,0,1)$ and $(0, 0, -1)$. (b) The (x, z)-plane cross-sectional plot of the asymptotic MFPT (2.5) in the case of two traps.

where the interaction energy term $\mathcal{H}(x_1, \dots, x_N)$ is

$$\mathcal{H}(x_1, \dots, x_N) = \sum_{i=1}^{N} \sum_{j=i+1}^{N} h(x_i; x_j), \qquad (2.9)$$

and the pairwise interaction energy is given by

$$h(x_i; x_j) = \frac{1}{|x_i - x_j|} - \frac{1}{2} \log |x_i - x_j| - \frac{1}{2} \log(2 + |x_i - x_j|).$$
$$(2.10)$$

The leading order behavior of the solution (2.5), (2.6), and (2.8) of the singular perturbation problem (1.1) is $O(N\epsilon^{-1})$, inversely proportional to the total trap area. The terms $O(\epsilon^0)$ explicitly depend on trap positions; in the formulas for the asymptotic average MFPT $\bar{v}$, these terms, having the form of total pairwise trap interaction energy (2.9), can be optimized by adjusting trap locations that minimize average escape times $\bar{v}$, thus producing optimal trap arrangements. (For some properties of such optimal arrangements, optimization techniques, and numerical solutions; see, e.g., Refs. [14–16,35] and references therein.)

A typical shape of the MFPT $v(x)$ for a unit sphere domain with two traps of size $\epsilon = 0.01$ located at one and both the poles, computed for the diffusivity $D = 1$, is shown in Fig. 2. While away from the traps, the asymptotic formula (2.5) provides a precise description of the solution of the problem (1.1) [16]; there is a significant difference near the traps ($|x - x_j| = O(\epsilon)$). In particular, the exact solution $v(x) \to 0$ when x approaches a trap x_j, and the asymptotic solution tends to negative infinity through the singularity behavior of Green's function (2.3).

Explicit formulas for the average MFPT in the case of two sets of traps on the boundary of the unit sphere, with radii $a_j = \epsilon$ for $j = 1, \dots, N$ and $a_j = \alpha\epsilon$ for $j = N + 1, \dots, 2N$, as well as some MFPT-minimizing configurations of such traps, were computed in Ref. [16].

B. Simulated Brownian motion

The Brownian motion was modeled by a continuous Wiener process with independent random time increments [8]. The path of a Brownian particle in this model is given by

the summation of the initial position and a series of normally distributed random displacements:

$$x_0 = x; \quad x_{n+1} = x_n + \Delta x_n, \quad n \geqslant 0; \qquad (2.11a)$$
$$\Delta x_n = \sqrt{3D\tau} \, \gamma_{n-1}; \quad \gamma_n \sim \mathcal{N}(0, 1). \qquad (2.11b)$$

where τ is the time increment. The MATLAB function `randn` is used to compute the normally distributed displacements. The MATLAB-based parallel code simulates runs of $N \gg 1$ Brownian particles, until each particle escapes the spherical domain through a boundary trap [see Fig. 3(a)].

For each simulated Brownian trajectory, when the particle is about to intersect the domain boundary (that is, $|x_n| < \epsilon$ and $|x_{n+1}| \geqslant \epsilon$), the intersection point q ($|q| = 1$) and the reflected position $\tilde{x}_n$ are computed [see Fig. 3(b)]. One explicitly calculates $\tilde{x}_n$ using basic trigonometry. In particular, for the boundary intersection point, one has

$$q = x_n + \alpha \frac{\Delta x_n}{|\Delta x_n|}, \quad |q| = 1. \qquad (2.12)$$

In (2.12), the coefficient α is given by

$$\alpha = \sqrt{1 + \kappa^2 - |x_n|^2} - \kappa, \quad \kappa = \frac{x_n \cdot \Delta x_n}{|\Delta x_n|}.$$
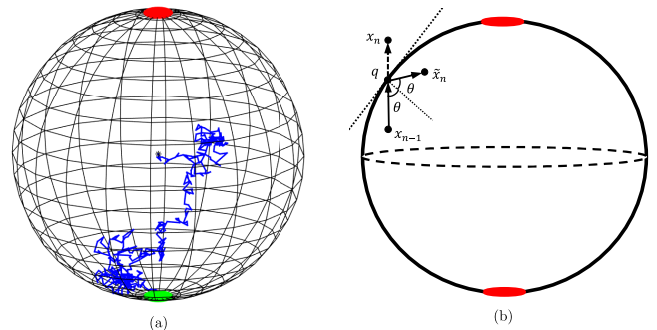

FIG. 3. (a) Schematics of a Brownian particle simulation in the unit sphere domain with two traps denoted by disks (top and bottom), leading to an escape through the bottom (green) trap. (b) Boundary reflection computation.
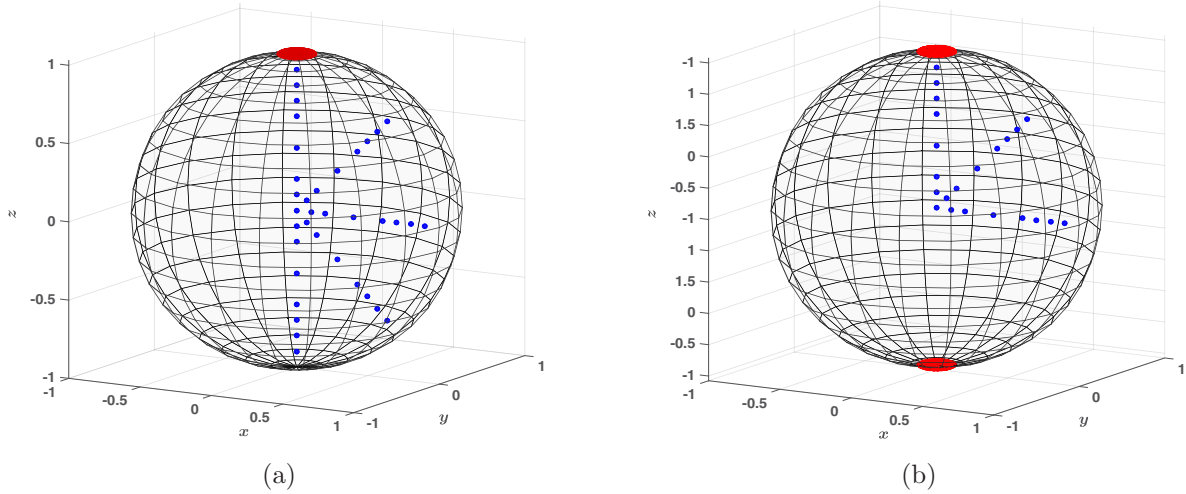
(a)   (b)

FIG. 4. Starting positions for Brownian launches for one-trap and two-trap unit sphere configurations.

The reflected position $\tilde{x}_n$ itself is found using the rotation matrix

$$\mathcal{R} = \begin{pmatrix} 2q_x^2 - 1 & 2q_x q_y & 2q_x q_z \\ 2q_y q_x & 2q_y^2 - 1 & 2q_y q_z \\ 2q_z q_x & 2q_z q_y & 2q_z^2 - 1 \end{pmatrix}$$

at q, and is given by

$$\tilde{x}_n = q - (\mathcal{R}\Delta x_n)\frac{|\Delta x_n| - |q - x_n|}{|\Delta x_n|}. \tag{2.13}$$

The particle escape condition through a trap of radius ϵ is based on the spherical arclength between the boundary intersection point q and the trap center at x_j:

$$\arccos(x_j \cdot q) \leqslant \epsilon.$$

In the simulated Brownian simulation, the time step was chosen to be $\tau = 6 \times 10^{-6}$, the trap size $\epsilon = 10^{-2}$, and the diffusivity $D = 1$ [without loss of generality by rescaling the PDE (1.1)]. For the number of particle runs for each starting location, it was determined that $N = 10^4$ is the optimal number in terms of sample size and running time. The dynamics was simulated in parallel, with a single thread dedicated to one particle, using the MATLAB `parfor` loop, on a 32-thread, 3.10 GHz Intel Xeon-based workstation with 128 GB memory. In this configuration, a typical computation for $N = 10^4$ particles launched from a single starting location takes between 5 and 10 hours, depending on the starting location.

C. Comparison of the asymptotic MFPT with the averaged Brownian escape times for various trap configurations

We now compare MFPT results from direct Brownian dynamics simulations with asymptotic MFPT (Sec. II). Three-dimensional trajectories of Brownian particles launched from points specified by (r, ϕ), the radial distance $0 \leqslant r \leqslant 1$ and a spherical angle ϕ, are computed until the escape of every particle through one of the traps. We first consider the simplest setup with a single trap of radius $\epsilon = 0.01$ located at the north pole $(0,0,1)$, and a two-trap configuration with the traps

of common radius $\epsilon = 0.01$ positioned at the poles $(0,0,1)$, $(0,0,-1)$ [Fig. 4(b)].

The Brownian average MFPT for a particle launched from x,

$$v_N^B(x) = \frac{1}{N}\sum_{i=1}^N v_i(x), \tag{2.14}$$

is computed by averaging single-particle escape times of N particles.

1. Single trap

For the single boundary trap located at the north pole $(0,0,1)$, Brownian particles were launched in the XZ-plane with starting positions $x = (r\sin\phi, 0, r\cos\phi)$ with

$$r = [0, 0.1, 0.2, 0.4, 0.6, 0.7, 0.8, 0.9],$$
$$\phi = \left[0, \frac{\pi}{4}, \frac{\pi}{2}, \frac{3\pi}{4}, \pi\right] \tag{2.15}$$

in terms of the spherical radius r and the spherical polar angle ϕ. Figure 5 shows the comparison between the asymptotic MFPT solution $v(x)$ (2.5) of the continuum problem (1.1) vs the Brownian-averaged MFPT $v_N^B(x)$ (2.14).

In order to measure the agreement between the Brownian-average and asymptotic MFPT values, define the relative difference between the two as

$$\delta v(x) = \frac{|v(x) - v_N^B(x)|}{v(x)} \times 100\%. \tag{2.16}$$

While the averaged Brownian simulation-based MFPT results theoretically require a "large" number launches N to agree with asymptotic formulas, we found that already at $N = 10^4$ particle runs from every starting point, the agreement is rather accurate, with $\delta v(x) \leqslant 1\%$ in most of the domain, achieving the maximum of 3% for the point $(0,0,0.9)$ closest to the trap located at $(0,0,1)$, where the accuracy of the asymptotic formula (2.5) already begins to deteriorate. Numerical values of $\delta v(x)$ are presented in Table I, and the line and contour plots of $\delta v(x)$ (2.16) are shown in Fig. 6.
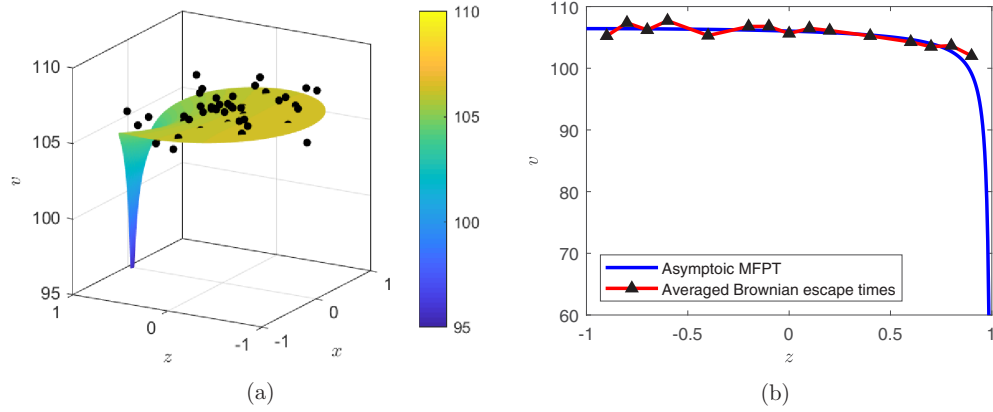
(a)

(b)

FIG. 5. (a) Scatter plot of the run-averaged Brownian escape times $v_N^B(x)$ (2.14) for various launching coordinates in XZ-plane, and the surface plot of the asymptotic MFPT $v(x)$ (2.5), for the one-trap configuration. (b) Comparison of Brownian MFPT $v_N^B(x)$ and asymptotic MFPT $v(x)$ along the Z-axis.

TABLE I. Brownian-average escape times $v_N^B(x)$ and their relative difference $\delta v(x)$ with the asymptotic MFPT results $v(x)$ (2.5) in the unit sphere with a single trap and two polar traps.

|	Averaged Brownian escape times		δv	
(r, ϕ)	One-trap	Two-trap	One-trap	Two-trap
$(0, 0)$	105.6267	52.8241	0.3745	0.1473
$(0.1, 0)$	106.4793	52.6118	0.5348	0.2495
$(0.2, 0)$	106.1091	52.7475	0.3149	0.0254
$(0.4, 0)$	105.2495	52.6111	0.1261	0.1509
$(0.6, 0)$	104.2623	52.9296	0.3784	0.6519
$(0.7, 0)$	103.4924	52.3500	0.4739	0.2502
$(0.8, 0)$	103.6674	52.0311	0.9282	0.4668
$(0.9, 0)$	102.0075	51.5775	2.9119	0.2003
$(0.1, \pi/4)$	106.5675	52.4829	0.5833	0.4975
$(0.2, \pi/4)$	106.8009	52.9024	0.8802	0.3037
$(0.4, \pi/4)$	104.9331	52.8041	0.7260	0.1381
$(0.6, \pi/4)$	104.9480	53.0296	0.5725	0.5901
$(0.7, \pi/4)$	106.3650	52.8598	0.8208	0.2779
$(0.8, \pi/4)$	105.8812	53.2618	0.3958	1.0478
$(0.9, \pi/4)$	106.8603	52.6601	1.3400	0.0884
$(0.1, \pi/2)$	106.6579	53.0176	0.5958	0.5126
$(0.2, \pi/2)$	106.9766	53.0463	0.8896	0.5627
$(0.4, \pi/2)$	105.8399	53.5098	0.2051	1.4258
$(0.6, \pi/2)$	106.9358	52.5211	0.8016	0.4658
$(0.7, \pi/2)$	107.3109	52.5139	1.1437	0.4870
$(0.8, \pi/2)$	106.0947	52.5367	0.0116	0.4498
$(0.9, \pi/2)$	105.5033	53.3428	0.5746	1.0738
$(0.1, 3\pi/4)$	106.4983		0.3843	
$(0.2, 3\pi/4)$	105.9568		0.1815	
$(0.4, 3\pi/4)$	105.7599		0.4550	
$(0.6, 3\pi/4)$	106.9267		0.5830	
$(0.7, 3\pi/4)$	106.3211		0.0060	
$(0.8, 3\pi/4)$	107.4246		1.0540	
$(0.9, 3\pi/4)$	107.2201		0.8164	
$(0.1, \pi)$	106.7835		0.6305	
$(0.2, \pi)$	106.7765		0.5533	
$(0.4, \pi)$	105.2995		0.9409	
$(0.6, \pi)$	107.7019		1.2518	
$(0.7, \pi)$	106.2090		0.1734	
$(0.8, \pi)$	107.3674		0.9004	
$(0.9, \pi)$	105.2420		1.1050	
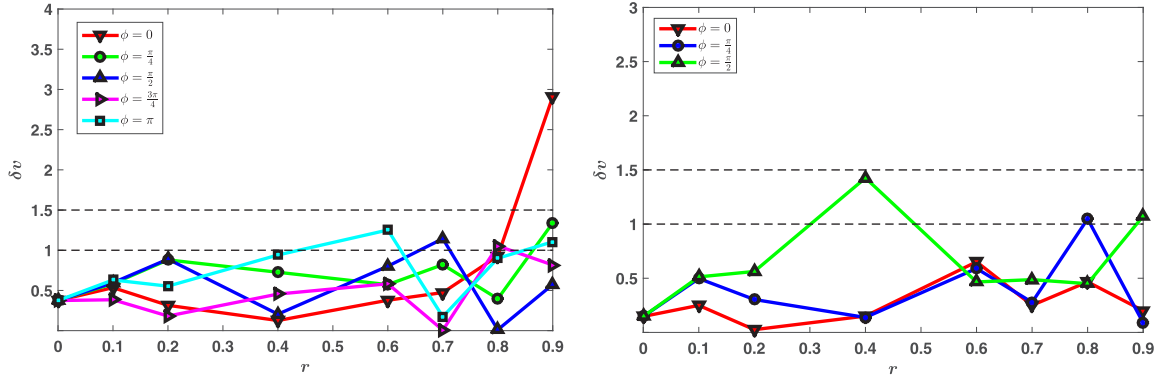
FIG. 6. Line plots for the relative percentage difference $\delta v(x)$ (2.16) for various starting locations in (a) one-trap and (b) two-trap configuration.

2. Two traps

For the two-trap setup shown in Fig. 4(b), due to the reflection symmetry, starting positions specified by spherical radii and spherical polar angles

$$r = [0, 0.1, 0.2, 0.4, 0.6, 0.7, 0.8, 0.9], \quad \phi = \left[0, \frac{\pi}{4}, \frac{\pi}{2}\right]$$

(2.17)

were used. The values of averaged Brownian escape times $v_N^B(x)$ (2.14) and their relative percentage differences δv with the asymptotic MFPT values $v(x)$ (2.5) are listed in Table I. Figure 7 provides a visual comparison of the Brownian and the asymptotic MFPTs, while the relative difference $\delta v(x)$ (2.16) between the two is shown in Fig. 6(b) (see also Table I); it does not exceed 1.5%.

3. The number of launches and Brownian simulation accuracy

We now compare the previous run results with $N = 10^4$ and a computation for $N = 10^3$, for 11 starting positions along the Z-axis. The averaged Brownian MFPT values for $N = 10^3$ and the relative difference values δv (2.16) are listed in Table II, and are compared with the data for $N = 10^4$ (listed in Table I) in Fig. 8. It is evident that the agreement between

asymptotic and Brownian-averaged MFPT significantly worsens for the smaller number of launches, reaching up to ~9%.

III. BROWNIAN DYNAMICS NEAR THE BOUNDARY

In contrast with the continuum approximation (1.1) of the narrow escape problems that does not preserve the single-particle trajectory data, direct Brownian simulations contain all such information. Reviewing Brownian paths of the particles from the starting point to the escape through the boundary trap, it is apparent that some particles spend a significant amount of their lifetime in a narrow region near the boundary, which may be defined as

$$\Omega_\delta = \{x \in \Omega \,|\, |x - 1| \leqslant \delta\},$$

(3.1)

where $a < \delta \ll |\Omega|$ is a small parameter independent of ϵ (see Fig. 9) and exceeding the typical Brownian particle size a. We use simulation data obtained above to estimate the fraction $\delta t = \delta t(x, \delta)$ of the dimensionless time the particle spends in Ω_δ, averaged over N particle launches from each starting location:

$$\delta t = \left\langle \frac{T_\delta}{T} \right\rangle.$$
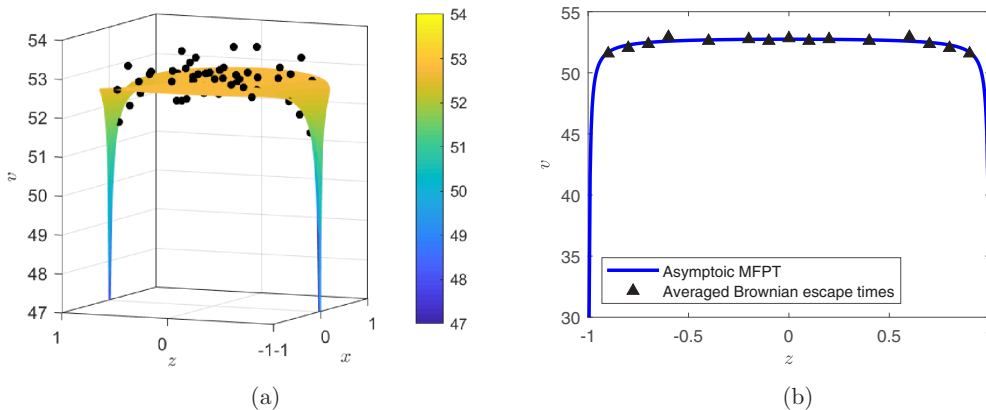
(3.2)

FIG. 7. (a) Scatter plot of the run-averaged Brownian escape times $v_N^B(x)$ (2.14) for various launching coordinates in XZ-plane, and the surface plot of the asymptotic MFPT $v(x)$ (2.5), for the two-trap configuration. (b) Comparison of Brownian MFPT $v_N^B(x)$ and asymptotic MFPT $v(x)$ along the Z-axis.

TABLE II. Brownian-average escape times $v_N^B(x)$ and their relative difference $\delta v(x)$ in the unit sphere with a single trap for 10^3 runs.

(r, ϕ)	Averaged Brownian MFPT	δv
$(0.9, \pi)$	104.3833	1.9078
$(0.8, \pi)$	108.5066	1.971
$(0.7, \pi)$	103.7186	2.5142
$(0.6, \pi)$	107.3154	0.8884
$(0.4, \pi)$	104.6452	1.5564
$(0.2, \pi)$	109.1458	2.7845
$(0.1, \pi)$	103.8133	2.1639
$(0.0, \pi)$	107.9336	1.8013
$(0.1, \pi)$	105.0048	0.8574
$(0,2)$	114.9412	8.6647
$(0.4,0)$	106.6409	1.1942
$(0.6,0)$	99.1448	5.2681
$(0.7,0)$	105.7482	1.6954
$(0.8,0)$	106.5300	3.7152
$(0.9,0)$	106.1181	7.0589

Here $T = n\tau$ represents the total time spent by the Brownian particle before an escape through one of the absorbing traps, in terms of the unit time step τ and the number of steps n before the escape, and $T_\delta = n_\delta \tau$ is the same measure of the total time spent by the particle in the Ω_δ boundary region. We compute δt as a function of launching coordinates (r, ϕ) for both the one-trap and the two-trap configurations.

For the domain with a single trap, with the trap is located at the north pole $x = (0, 0, 1)$, we calculated the boundary time fraction δt (3.2) spent by Brownian particles in boundary regions of thicknesses $\delta = 0.1$ and $\delta = 0.01$, averaged over for $N = 10^4$ launches from each of the starting positions. The same computation was done for the two-trap configuration where the traps were placed at the north pole $(0,0,1)$ and the south pole $(0, 0, -1)$. The results are visualized in Figs. 10 and 11 with numerical details in Table III.

For $\delta = 0.1$, which corresponds to Ω_δ occupying $\sim 27.1\%$ of the total volume of the spherical domain, $\delta t \simeq 28.18\%$ was
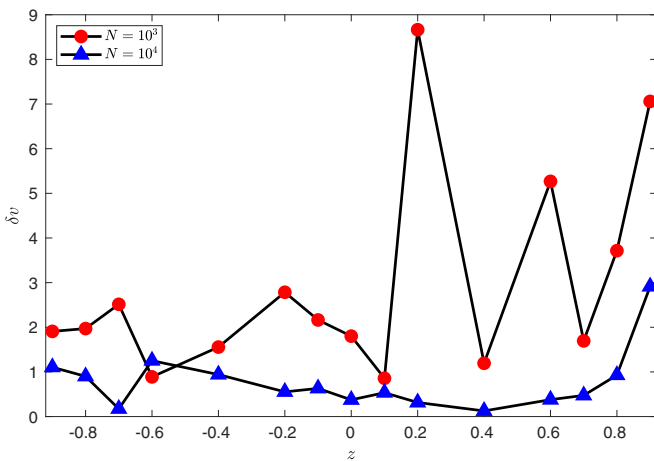

FIG. 8. Relative percent difference $\delta v(x)$ (2.16) between Brownian and asymptotic MFPT in the one-trap configuration for $N = 10^3$ vs $N = 10^4$ Brownian launches.
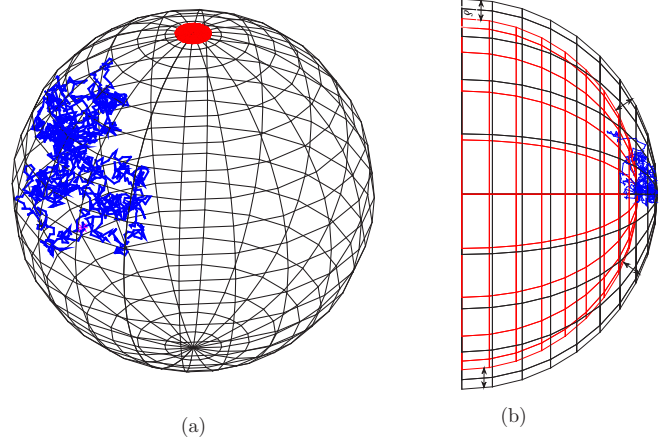

FIG. 9. (a) Sample dynamics of a Brownian particle near the boundary. (b) The δ-region Ω_δ near the domain boundary.

approximately constant throughout the range of launching positions. According to the column average values of Table III, for $\delta = 0.01$, corresponding to a boundary layer occupying $\sim 2.97\%$ of the total volume of the sphere, the particles spent around $\delta t \simeq 3.99\%$ within the δ-region of the boundary. This independence of launching positions is consistent with the fact that the relative boundary time characterizes Brownian motion rather than a narrow escape problem. [For launching positions located near the trap (Fig. 10), the boundary time fraction is higher because of higher absorption rate and smaller chance of the particle to move freely in the domain.]

The values of relative boundary times δt computed for the two-trap configuration, for most of the starting positions within the bulk of the domain, were found to be almost identical to those for the single-trap configuration. The comparative data is presented in Table IV (here figures are given with higher precision than in Table III).

Importantly, for both values of the boundary layer thickness δ, particles spent near the boundary longer than predicted by the relative volume of the boundary layer: $\delta t > |\Omega_\delta|/|\Omega|$, being more evident for $\delta = 0.01$, where

$$\delta t \simeq 1.34 \frac{|\Omega_\delta|}{|\Omega|}. \tag{3.3}$$

IV. COMPARISON OF BROWNIAN DYNAMICS SIMULATIONS FOR ANISOTROPIC AND ISOTROPIC DIFFUSIONS

In Sec. III it has been demonstrated that in the assumption of constant isotropic diffusion D throughout the domain, particles undergoing simulated Brownian motion spend relatively more time of their travel in the narrow boundary region. There are, however, further boundary effects that can be taken into account in such simulations and can contribute to even more highly altered boundary dynamics, in particular, effects of anisotropic near-boundary diffusion.

According to Stokes' law, a spherical particle of radius a traveling with velocity v in a quiescent fluid in an unbounded domain experiences the hydrodynamic drag force $F_0 = -6\pi \eta a v$, where η is fluid's viscosity. The corresponding ambient diffusivity is expressed by the Stokes-Einstein
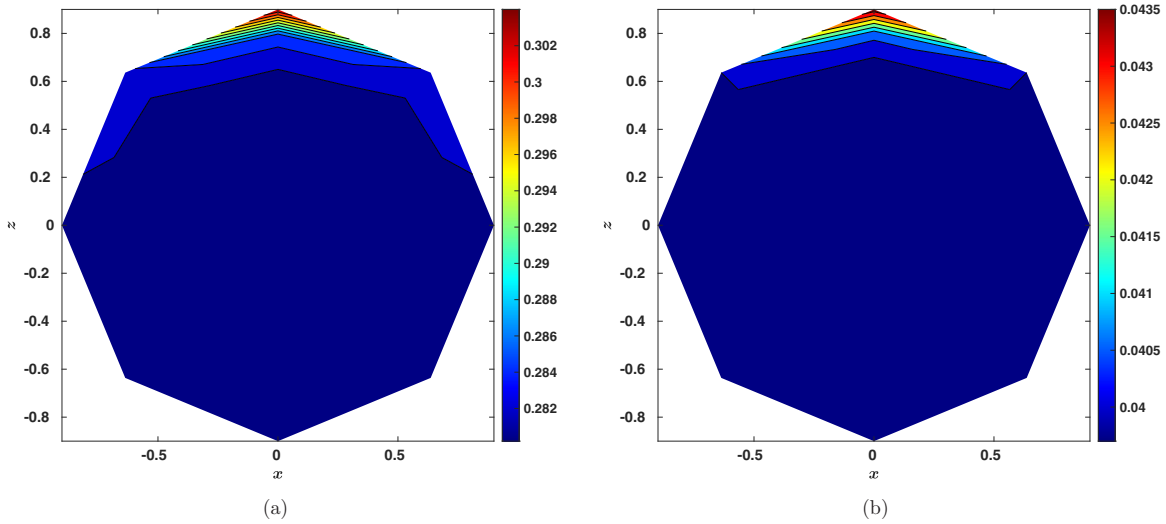
(a)　　　　　　　　　　　　　　　　(b)

FIG. 10. Contour plots of the averaged relative boundary time δt (3.2) spent by Brownian particles in the boundary layer Ω_δ for the narrow escape problem in a sphere with a single trap and starting positions (2.15), for the boundary layer width (a) $\delta = 0.1$ and (b) $\delta = 0.01$. Full data in Table III.

relation

$$D_0 = \frac{k_B T}{6\pi \eta a},$$

where k_B is the Boltzmann constant, and T is the temperature of the system. The presence of a boundary wall alters the domain and the drag force, since the fluid flow has to satisfy additional boundary conditions. This results in different drag forces in the direction parallel and perpendicular to the wall; these forces can be represented as scaled versions of F_0,

$$F_\parallel = \lambda_\parallel F_0, \quad F_\perp = \lambda_\perp F_0,$$

in terms of unknown factors $\lambda_\parallel$ and $\lambda_\perp$, and correspond to anisotropic diffusivity components:

$$D_\parallel = \frac{k_B T}{6\pi \eta a \lambda_\parallel} = \lambda_\parallel^{-1} D_0, \quad D_\perp = \frac{k_B T}{6\pi \eta a \lambda_\perp} = \lambda_\perp^{-1} D_0. \tag{4.1}$$

(In this work, we continue to assume $D_0 = D = 1$, which can be achieved through a rescaling of the problem.) The exact solution for $\lambda_\perp$ for a particle of radius a located at the distance z from the domain boundary was computed in Ref. [36] in the form of a series of $\lambda_\perp^{-1}$ in powers of (a/z). In fact, an iterative method of reflections [26] allows to successively calculate both the first terms of the series for $\lambda_\perp^{-1}$ and the leading terms of a similar power series for $\lambda_\parallel^{-1}$ near a flat wall.
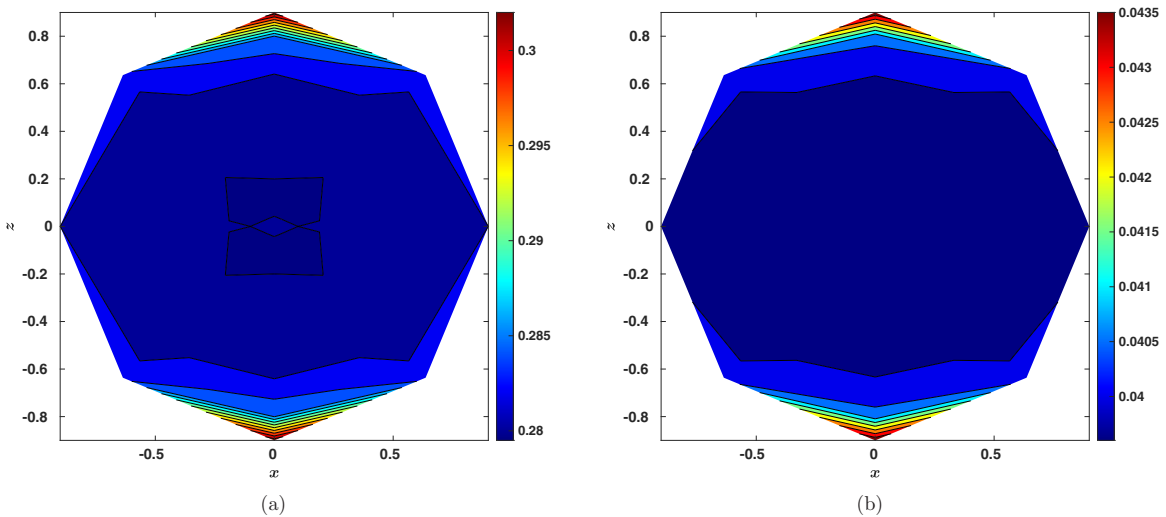

(a)　　　　　　　　　　　　　　　　(b)

FIG. 11. Contour plots of the averaged relative boundary time δt (3.2) spent by Brownian particles in the boundary layer Ω_δ for the narrow escape problem in a sphere with two traps and starting positions (2.17), for the boundary layer width (a) $\delta = 0.1$ and (b) $\delta = 0.01$. Full data in Table III.

TABLE III. Average boundary time fraction values δt (3.2) for a Brownian particle in the unit sphere with a single trap of radius $\epsilon = 0.01$ as a function of the starting position (r, ϕ) in the XZ-plane (r is the spherical radius, and ϕ is the polar angle measured from the Z-axis).

| | Boundary time fraction δt | | | |
| | $\delta = 0.1$ | | $\delta = 0.01$ | |
(r, ϕ)	One-trap	Two-trap	One-trap	Two-trap
$(0, 0)$	0.2804	0.2803	0.0397	0.0397
$(0.1, 0)$	0.2808	0.2796	0.0398	0.0396
$(0.2, 0)$	0.2802	0.2800	0.0397	0.0397
$(0.4, 0)$	0.2809	0.2801	0.0398	0.0397
$(0.6, 0)$	0.2816	0.2811	0.0399	0.0399
$(0.7, 0)$	0.2824	0.2833	0.0400	0.0402
$(0.8, 0)$	0.2861	0.2859	0.0407	0.0407
$(0.9, 0)$	0.3040	0.3032	0.0438	0.0439
$(0.1, \pi/4)$	0.2803	0.2796	0.0397	0.0396
$(0.2, \pi/4)$	0.2806	0.2795	0.0397	0.0396
$(0.4, \pi/4)$	0.2805	0.2806	0.0397	0.0397
$(0.6, \pi/4)$	0.2812	0.2811	0.0398	0.0398
$(0.7, \pi/4)$	0.2817	0.2815	0.0399	0.0399
$(0.8, \pi/4)$	0.2823	0.2820	0.0400	0.0400
$(0.9, \pi/4)$	0.2826	0.2828	0.0400	0.0401
$(0.1, \pi/2)$	0.2803	0.2800	0.0397	0.0397
$(0.2, \pi/2)$	0.2804	0.2801	0.0397	0.0397
$(0.4, \pi/2)$	0.2810	0.2802	0.0398	0.0397
$(0.6, \pi/2)$	0.2809	0.2805	0.0398	0.0397
$(0.7, \pi/2)$	0.2810	0.2812	0.0398	0.0398
$(0.8, \pi/2)$	0.2817	0.2817	0.0399	0.0399
$(0.9, \pi/2)$	0.2817	0.2820	0.0399	0.0399
$(0.1, 3\pi/4)$	0.2807		0.0398	
$(0.2, 3\pi/4)$	0.2808		0.0398	
$(0.4, 3\pi/4)$	0.2809		0.0398	
$(0.6, 3\pi/4)$	0.2809		0.0398	
$(0.7, 3\pi/4)$	0.2812		0.0398	
$(0.8, 3\pi/4)$	0.2814		0.0399	
$(0.9, 3\pi/4)$	0.2816		0.0399	
$(0.1, \pi)$	0.2806		0.0398	
$(0.2, \pi)$	0.2803		0.0397	
$(0.4, \pi)$	0.2808		0.0398	
$(0.6, \pi)$	0.2809		0.0398	
$(0.7, \pi)$	0.2812		0.0398	
$(0.8, \pi)$	0.2815		0.0399	
$(0.9, \pi)$	0.2816		0.0399	
Average δt	0.2818	0.2821	0.0400	0.0400

TABLE IV. Average boundary time fraction values δt (3.2) vs volume fraction of the boundary region in the case of isotropic diffusion of Brownian particles in the unit sphere with one and two polar traps of radius $\epsilon = 0.01$, for boundary layer thicknesses $\delta = 0.1$ and $\delta = 0.01$.

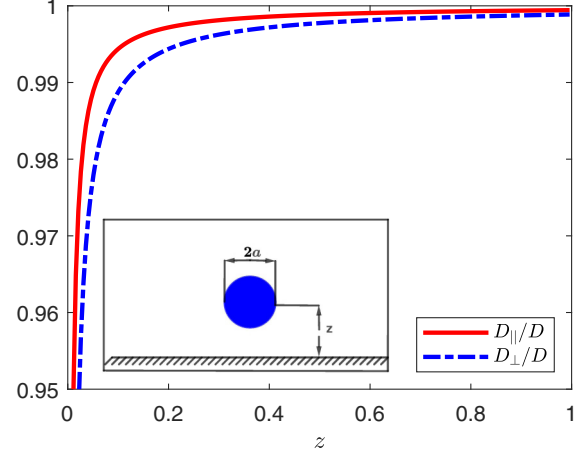| δ	Boundary layer volume fraction $\|\Omega_\delta\|/\|\Omega\|$	δt, single-trap	δt, two-trap
0.1	27.10%	28.18%	28.21%
0.01	2.970%	3.995%	4.002%

FIG. 12. Relative anisotropic diffusion coefficients $D_\parallel/D$ and $D_\perp/D$ (4.1) a Brownian particle of radius $a = 0.001$ as functions of the distance z from the domain wall.

The expansions for the dimensionless anisotropy coefficients given in Ref. [26] read

$$\lambda_\parallel^{-1} \simeq 1 - \frac{9}{16}\left(\frac{a}{z}\right) + \frac{1}{8}\left(\frac{a}{z}\right)^3 - \frac{45}{256}\left(\frac{a}{z}\right)^4$$
$$- \frac{1}{16}\left(\frac{a}{z}\right)^5 + O\left(\frac{a}{z}\right)^6, \tag{4.2a}$$

$$\lambda_\perp^{-1} \simeq 1 - \frac{9}{8}\left(\frac{a}{z}\right) + \frac{1}{2}\left(\frac{a}{z}\right)^3 + O\left(\frac{a}{z}\right)^4. \tag{4.2b}$$

The expansions (IV.2) were experimentally verified in Ref. [25] using direct microscopy-based measurements.

Near the boundary, $D_\perp < D_\parallel < D$ (Fig. 12), and the diffusivities $D_\perp, D_\parallel$ approach $D_0 = 1$ as $a/z \to 0$. In particular, both $D_\perp, D_\parallel > 0.95 D$ for $z \gtrsim 22.5\,a$.

To model anisotropic diffusion, the MATLAB code was modified to decompose Brownian path increments (2.11b) into components parallel and perpendicular to the spherical boundary, and these components were rescaled separately according to (4.1). The code was run with particle sizes $a = 0.001$, with the goal to recompute the results of Secs. II and III, that is, Brownian-averaged MFPT times and boundary time fractions for one- and two-trap spherical configurations, in order to observe anisotropic diffusion effects.

A. Averaged Brownian escape times with anisotropic diffusion

In the anisotropic diffusion framework with parameters listed above, for the unit sphere with a single trap located at the north pole $Z = 1$, starting positions along the Z-axis, and $\sim 1.3 \times 10^4$ runs from each starting location, the averaged Brownian MFPT values (2.14) are listed in Table V. Figure 13 compares these averaged Brownian escape times for the anisotropic diffusion case with the MFPT values obtained from the corresponding Brownian simulations and the asymptotic MFPT for isotropic diffusion (cf. Sec. II C, Fig. 5). It can be observed that in the case of variable diffusion, the escape times are about 10% smaller, which is overall an expected result since because near the boundary, the anisotropic diffusivity coefficients are lower than the ambient diffusivity

TABLE V. Averaged Brownian MFPT values $v_N^B(x)$ (2.14) in the case of anisotropic diffusion with diffusivity coefficients (4.1).

(r, ϕ)	Averaged Brownian MFPT
$(0.9, \pi)$	94.1280
$(0.8, \pi)$	90.1409
$(0.7, \pi)$	93.7804
$(0.6, \pi)$	92.7116
$(0.5, \pi)$	94.4702
$(0.4, \pi)$	94.7872
$(0.3, \pi)$	93.6790
$(0.2, \pi)$	93.5953
$(0.1, \pi)$	95.1294
$(0,0)$	92.6663
$(0.1,0)$	96.8617
$(0.2,0)$	92.4898
$(0.3,0)$	90.9424
$(0.4,0)$	94.0706
$(0.5,0)$	92.5329
$(0.6,0)$	90.1264
$(0.7,0)$	90.8989
$(0.8,0)$	89.2767
$(0.9,0)$	90.1289

D_0. As we will see below, this also has to do with the fact that for the anisotropic diffusion model, the time spent by particles near the walls is also greater than in the isotropic case.

B. Boundary times with anisotropic diffusion

Similarly to the work done in Sec. III above, the simulated Brownian trajectories computed above in the anisotropic setting can be used to calculate boundary time fraction δt (3.2) spent in the δ-neighborhood (3.1) of the boundary. For $\delta = 0.1$ and $\delta = 0.01$, and $\sim 1.3 \times 10^4$ launches from each starting position, the results are presented in Table VI, and compared with isotropic diffusion boundary time fraction in Fig. 14.

From the comparison in Fig. 14 and between Tables III and VI, it is evident that in the anisotropic case, the particles on average spend more time at the boundary. This time fraction
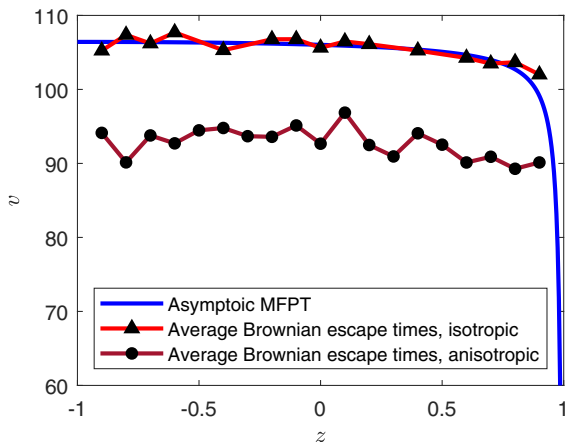

FIG. 13. Averaged Brownian MFPT values (2.14) for anisotropic and isotropic diffusion vs the asymptotic MFPT $v(x)$ (2.5) for particle launch locations along the Z-axis (see also Fig. 5).

TABLE VI. Average boundary time fraction values δt (3.2) for a Brownian particle in the unit sphere with a single trap of radius $\epsilon = 0.01$ in the case of anisotropic diffusion with diffusivity coefficients (4.1), as a function of the starting position (r, ϕ) in the XZ-plane.

(r, ϕ)	Boundary time fraction δt	
	$\delta = 0.1$	$\delta = 0.01$
$(0.9, \pi)$	0.2841	0.0438
$(0.8, \pi)$	0.2842	0.0439
$(0.7, \pi)$	0.2842	0.0439
$(0.6, \pi)$	0.2842	0.0439
$(0.5, \pi)$	0.2834	0.0438
$(0.4, \pi)$	0.2832	0.0437
$(0.3, \pi)$	0.2830	0.0437
$(0.2, \pi)$	0.2830	0.0437
$(0.1, \pi)$	0.2830	0.0437
$(0,0)$	0.2829	0.0437
$(0.1,0)$	0.2831	0.0437
$(0.2,0)$	0.2838	0.0438
$(0.3,0)$	0.2836	0.0438
$(0.4,0)$	0.2831	0.0437
$(0.5,0)$	0.2832	0.0437
$(0.6,0)$	0.2848	0.0041
$(0.7,0)$	0.2857	0.0442
$(0.8,0)$	0.2885	0.0449
$(0.9,0)$	0.3088	0.0481
Average δt	0.2853	0.0441

is about 1% higher than in the isotropic case for $\delta = 0.1$, and about 10% higher than in the isotropic case for $\delta = 0.01$. The comparison with the boundary region volume fraction $|\Omega_\delta|/|\Omega|$ for both isotropic and anisotropic diffusion cases is presented in Table VII, which generalizes Table IV in the case of a single polar trap. (In Table VII, figures are given with higher precision than in Table VI.)

V. DISCUSSION AND CONCLUSIONS

The narrow escape problem of finding mean first-passage time $v(x)$ for a Brownian particle starting from a point x in a bounded domain Ω with traps can be computationally
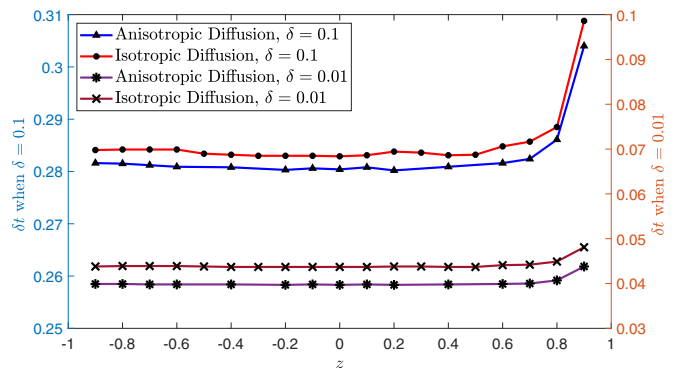

FIG. 14. Comparison of boundary time fraction values δt (3.2) for isotropic vs anisotropic diffusion for the boundary layer thickness $\delta = 0.1$ and $\delta = 0.01$.

TABLE VII. Average boundary time fraction values δt (3.2) vs volume fraction of the boundary region in the case of isotropic and anisotropic diffusion of Brownian particles in the unit sphere with a single polar trap of radius $\epsilon = 0.01$.

δ	Boundary layer volume fraction $\|\Omega_\delta\|/\|\Omega\|$	δt, isotropic	δt, anisotropic
0.1	27.10%	28.29%	28.53%
0.01	2.970%	4.014%	4.410%

approached directly through performing multiple simulations of Brownian trajectories $\{W(t)\}_{t \geqslant 0}$ until the time of escape and averaging these escape times, or through the solution (exact, approximate, or numerical) of the Poisson problem (1.1) that serves as a continuum approximation of the narrow escape problem.

The first goal of this work is to perform a direct numerical simulation of multiple particles undergoing Brownian motion in a spherical 3D domain with boundary traps, to compute MFPT values by averaging of Brownian escape times, and to compare the results with those predicted by approximate solutions of the singularly perturbed MFPT problem (1.1). The second goal is a better understanding of such aspects of the simulated escape kinetics as residence times near the boundary, which could not be extracted from asymptotic MFPT results since the latter retain no trajectory information. Efficient and flexible, fully parallelized MATLAB code was developed and tested for these purposes. This code and its modifications can be applied to study Brownian motion-based diffusion processes and their statistical characteristics in domains of various geometries and dimensionality. The current code simulates trajectories (2.11) of Brownian particles starting from a given point in a unit sphere up to their escape through a trap, taking into account boundary reflections in a rigorous way (Sec. II B).

The asymptotic MFPT solution describing the starting position-dependent and average MFPT for a unit sphere with N well-separated asymptotically small (size $\sim \epsilon$) absorbing traps on the surface is given by expressions (2.5) and (2.6). (These results have been compared to numerical solutions and validated for a broad range of ϵ values in Ref. [16].) In Sec. II C the asymptotic MFPT formulas were compared with the averaged Brownian escape times, for a sphere with one and two small traps, for $N = 10^4$ runs originating at a variety of starting positions x along the symmetry axis and in the equatorial plane, with results presented in Table I. The relative difference (2.16) between asymptotic and Brownian average MFPT values has been shown to mostly not exceed 1% (Figs. 5, 6, and 7). These results provide an additional independent validation, in terms of modeling and computation, of both the Poisson MFPT problem (1.1) and its asymptotic solution (2.5) and (2.6).

It is well known that Brownian particles tend to spend relatively more time near the domain wall than in the bulk (e.g., [22,23,31]). The narrow escape trajectory information obtained in Sec. II C was used in Sec. III to compute the time spent by the particles starting at different positions until their escape, in the δ-neighborhood $|\Omega_\delta|$ (3.1) of the spherical

boundary, for $\delta = 0.1$ and 0.01. The boundary time fraction (3.2) values given in Table III are fairly constant throughout the domain, with the exception of starting positions close to the traps and thus to the boundary region itself, which gives a particle smaller chances to travel in the domain bulk (Figs. 10 and 11). In Table IV average boundary time fraction values δt were compared to the volume fraction $|\Omega_\delta|/|\Omega|$ of the boundary region. It was observed that in each case, the relative boundary time $\delta t > |\Omega_\delta|/|\Omega|$, showing that Brownian particles indeed tend to "stick to the boundary" even in the case of a constant diffusion coefficient D. In particular, for the thinner boundary layer $\delta = 0.01$, the factor by which the relative time spent at the boundary exceeds the relative boundary layer volume reaches about 34% (see (3.3)). These findings resonate with the work in Ref. [22] where a three-dimensional anisotropic diffusion model described by stochastic differential equations was presented and studied using asymptotic analysis and probabilistic methods.

In Sec. IV Brownian simulations were extended to incorporate an anisotropic variable diffusivity model (12) acting essentially near the boundary, with diffusivity higher values in the direction tangent to the boundary and lower values in the normal direction, depending on the particle size to boundary distance ratio a/z [25]. For a spherical domain with a single polar trap of radius $\epsilon = 0.01$ and particle size $a = 0.001$, the escape statistics was recomputed and compared with that of the common constant-diffusion model of Sec. II C. Data in Table V and Fig. 13 show that the use of the extended diffusion model results in a significant (about 10%) decrease of MFPT values. This effect must be related to faster diffusion along the boundary, which results in more trajectory time spent in the boundary layer and a faster trap detection, as confirmed by the computed relative boundary times δt (Fig. 14 and Table VII). The latter are larger for the anisotropic model, in particular, for the thin boundary layer $\delta = 0.01$, the anisotropic relative boundary time is about 10% higher than that in the initial model with isotropic diffusion.

The code used in the computations for the present work is available for download [32]. The code can be modified in a straightforward manner to study Brownian dynamics for both the anisotropic and isotropic diffusion for domains of arbitrary shapes, including those for which no analytical MFPT results are available.

The Brownian simulation adopted in this work may be generalized through the use of a more general Langevin's velocity-based Brownian motion model, defined as the stochastic difference equation

$$\frac{x_{n+1} - x_n}{\Delta t} = v_n, \qquad \frac{v_{n+1} - v_n}{\Delta t} = -\frac{1}{\tau}\left(v_n - \frac{\Delta x_n}{\Delta t}\right), \quad (5.1)$$

where x_n and v_n represent the position and the velocity of the Brownian particle, τ is the characteristic timescale, and the normally distributed random displacement Δx_n is given by (2.11b). The Langevin model (5.1) can be written as a second-order difference equation

$$x_{n+1} = x_n + \left(1 - \frac{\Delta t}{\tau}\right)(x_n - x_{n-1}) + \frac{\Delta t}{\tau}(\Delta x_{n-1}). \quad (5.2)$$

When the time step Δt equals the relaxation time τ, Eq. (5.2) reduces to the Wiener process (2.11).

In future work it would be of interest to modify the continuum MFPT model (1.1) and the extended model of Sec. IV to include more general forms of variable and/or anisotropic diffusion in three dimensions, for example, through the use of a general diffusivity tensor, and ideally, develop generalizations of existing closed-form exact and approximate solutions available in the literature. The numerical algorithm presented in this paper can be naturally adapted to perform Brownian simulations for such models.

It is of interest to compare the extended diffusivity model adopted in Sec. IV of this work to a different approach involving variable diffusion, proposed in Ref. [27], where in a two-dimensional disk domain, the diffusion coefficient was chosen piecewise-constant in the radial direction, providing a simplified way to take into account, for example, effects of spatial organization of the cytoskeleton in biological cells. While belonging to the same general framework, the model (4.1) adopted in this study and the model of Ref. [27] are different in many ways, describing different physical situations. In particular, the first model is based on experimental studies of near-surface bulk diffusion aspects; it provides continuous expressions for two components of the anisotropic diffusivity tensor. The second model assumes a simple form of isotropic variable diffusion, which leads to interesting extensions of known analytical results and insights into the effects of variable diffusivity. Brownian-type simulations similar to ones performed in this work can be used to provide further insights in the settings of Ref. [27] and more general ones, for example, two- and three-dimensional symmetric domains with nonsymmetric diffusivity variations.

Other directions of future research based on simulated Brownian motion can involve further generalizations of the current algorithm to include purely surface-mediated diffusion and the resulting two-state paths of Brownian particles, which would allow to compute simulated transition rates between the surface and the bulk of the domain, account for imperfect boundary adsorption and other effects, thus providing a context for comparison with multiple theoretical results in the area, such as those presented in Refs. [30,31] and references therein. As a related application, it is also interesting to perform direct Brownian simulations in more complex physical settings, including moving receptors on the surface of the domain [22] and the presence of force fields modeling forced diffusion [29].

[1] Z. Schuss, A. Singer, and D. Holcman, The narrow escape problem for diffusion in cellular microdomains, Proc. Nat. Acad. Sci. USA **104**, 16098 (2007).

[2] D. Holcman and Z. Schuss, Escape through a small opening: Receptor trafficking in a synaptic membrane, J. Stat. Phys. **117**, 975 (2004).

[3] I. V. Grigoriev, Y. A. Makhnovskii, A. M. Berezhkovskii, and V. Y. Zitserman, Kinetics of escape through a small hole, J. Chem. Phys. **116**, 9574 (2002).

[4] M. J. Skaug, L. Wang, Y. Ding, and D. K. Schwartz, Hindered nanoparticle diffusion and void accessibility in a three-dimensional porous medium, ACS Nano **9**, 2148 (2015).

[5] S. A. Gorski, M. Dundr, and T. Misteli, The road much traveled: Trafficking in the cell nucleus, Curr. Opin. Cell Biol. **18**, 284 (2006).

[6] G. Oshanin, O. Vasilyev, P. L. Krapivsky, and J. Klafter, Survival of an evasive prey Proc. Nat. Acad. Sci. USA **106**, 13696 (2009).

[7] S. Redner, *A Guide to First-Passage Processes* (Cambridge University Press, Cambridge, 2001).

[8] S. Heinz, *Mathematical Modeling* (Springer, Berlin, 2011).

[9] A. Singer, Z. Schuss, and D. Holcman, Narrow escape and leakage of Brownian particles, Phys. Rev. E **78**, 051111 (2008).

[10] A. Singer, Z. Schuss, and D. Holcman, Narrow escape, part II: The circular disk, J. Stat. Phys. **122**, 465 (2006).

[11] S. Pillay, M. Ward, A. Peirce, and T. Kolokolnikov, An asymptotic analysis of the mean first passage time for narrow escape problems. Part I: Two-dimensional domains, Multiscale Model. Simul. **8**, 803 (2010).

[12] A. Cheviakov, M. Ward, and R. Straube, An asymptotic analysis of the mean first passage time for narrow escape problems. Part II: The sphere, Multiscale Model. Simul. **8**, 836 (2010).

[13] S. A. Iyaniwura, T. Wong, C. B. Macdonald, and M. J. Ward, Optimization of the mean first passage time in near-disk and elliptical domains in 2-D with small absorbing traps, SIAM Rev. **63**, 525 (2021).

[14] A. F. Cheviakov and D. Zawada, Narrow-escape problem for the unit sphere: Homogenization limit, optimal arrangements of large numbers of traps, and the N^2 conjecture, Phys. Rev. E **87**, 042118 (2013).

[15] W. J. M. Ridgway and A. F. Cheviakov, Locally and globally optimal configurations of N particles on the sphere with applications in the narrow escape and narrow capture problems, Phys. Rev. E **100**, 042413 (2019).

[16] A. F. Cheviakov, A. S. Reimer, and M. J. Ward, Mathematical modeling and numerical computation of narrow escape problems, Phys. Rev. E **85**, 021131 (2012).

[17] D. Gomez and A. F. Cheviakov, Asymptotic analysis of narrow escape problems in nonspherical three-dimensional domains, Phys. Rev. E **91**, 012137 (2015).

[18] X. Li, Matched asymptotic analysis to solve the narrow escape problem in a domain with a long neck, J. Phys. A: Math. Theor. **47**, 505202 (2014).

[19] J. C. Tzou, S. Xie, and T. Kolokolnikov, First-passage times, mobile traps, and Hopf bifurcations, Phys. Rev. E **90**, 062138 (2014).

[20] J. C. Tzou and T. Kolokolnikov, Mean first passage time for a small rotating trap inside a reflective disk, Multiscale Model. Simul. **13**, 231 (2015).

[21] A. J. Bernoff and A. E. Lindsay, Numerical approximation of diffusive capture rates by planar and spherical surfaces with absorbing pores, SIAM J. Appl. Math. **78**, 266 (2018).

[22] S. D. Lawley and C. E. Miles, How receptor surface diffusion and cell rotation increase association rates, SIAM J. Appl. Math. **79**, 1124 (2019).

[23] S. D. Lawley and C. E. Miles, Diffusive search for diffusing targets with fluctuating diffusivity and gating, J. Nonlinear Sci. **29**, 2955 (2019).

[24] S. D. Lawley, A. E. Lindsay, and C. E. Miles, Receptor Organization Determines the Limits of Single-Cell Source Location Detection, Phys. Rev. Lett. **125**, 018102 (2020).

[25] B. Lin, J. Yu, and S. A. Rice, Direct measurements of constrained Brownian motion of an isolated sphere between two walls, Phys. Rev. E **62**, 3909 (2000).

[26] J. Happel and H. Brenner, *Low Reynolds Number Hydrodynamics, with Special Applications to Particulate Media* (Prentice-Hall, New York, 1983).

[27] M. Mangeat and H. Rieger, The narrow escape problem in a circular domain with radial piecewise constant diffusivity, J. Phys. A: Math. Theor. **52**, 424002 (2019).

[28] O. Bénichou, C. Loverdo, M. Moreau, and R. Voituriez, Intermittent search strategies, Rev. Mod. Phys. **83**, 81 (2011).

[29] T. Lagache and D. Holcman, Effective motion of a virus trafficking inside a biological cell, SIAM J. Appl. Math. **68**, 1146 (2008).

[30] F. Rojo and C. E. Budde, Enhanced diffusion through surface excursion: A master-equation approach to the narrow-escape-time problem, Phys. Rev. E **84**, 021117 (2011).

[31] J.-F. Rupprecht, O. Bénichou, D. S. Grebenkov, and R. Voituriez, Kinetics of active surface-mediated diffusion in spherically symmetric domains, J. Stat. Phys. **147**, 891 (2012).

[32] V. Srivastava and A. Cheviakov, "Brownian dynamics simulations for the narrow escape problem in the unit sphere: Matlab code," https://github.com/afshevyakov/Brownian (2021).

[33] N. Lebedev, I. Skalskaya, and Y. Uflyand, *Worked Problems in Applied Mathematics* (Dover, New York, 1979).

[34] X. Chen and A. Friedman, Asymptotic analysis for the narrow escape problem, SIAM J. Math. Anal. **43**, 2542 (2011).

[35] W. J. Ridgway and A. F. Cheviakov, An iterative procedure for finding locally and globally optimal arrangements of particles on the unit sphere, Comput. Phys. Commun. **233**, 84 (2018).

[36] H. Brenner, The slow motion of a sphere through a viscous fluid towards a plane surface, Chem. Eng. Sci. **16**, 242 (1961).